A&A 413, 363–371 (2004)
DOI: 10.1051/0004-6361:20031510
© ESO 2003

Astronomy & Astrophysics

Coronal transients and metric type II radio bursts

I. Effects of geometry

S. Mancuso[1] and J. C. Raymond[2]

[1] Istituto Nazionale di Astrofisica (INAF), Osservatorio Astronomico di Torino, Strada Osservatorio 20, Pino Torinese 10025, Italy
[2] Harvard-Smithsonian Center for Astrophysics, 60 Garden Street, MS 50, Cambridge, MA 02138, USA

Received 16 June 2003 / Accepted 22 September 2003

Abstract. In this paper we investigate the relationship between type II and coronal transient activity in terms of emission originating from the top or the flanks of a bow/piston shock surface, extending just above the coronal mass ejection (CME) leading edge surface. For this purpose, we used ground-based metric type II radio burst observations of twenty-nine events in conjunction with Large Angle and Spectrometric Coronagraph (LASCO/SOHO) and UltraViolet Coronagraph Spectrometer (UVCS/SOHO) observations. With the refined density diagnostic offered by the UVCS instrument, we analyzed the type II dynamics in conjunction with the associated CME dynamics. Although we found some correlation, in all but a few cases the coronal transients appeared to lead the type II emission locations by several minutes, in apparent disagreement with a CME-driven origin interpretation. By applying a simple model, we found however that a piston-driven origin is certainly viable for all the events under study on the hypothesis that the radio emission originates in discrete locations above the top or the flanks of bow/piston shock surfaces extending just above the transient leading edges.

Key words. Sun: corona – UV radiation – radio radiation – coronal mass ejections – shock waves

1. Introduction

It is well known from spacecraft observations that essentially all decameter/hectometer type II emissions at the local electron plasma frequency and its harmonic are associated with shocks driven by fast and wide interplanetary coronal transients (Cane et al. 1987; Gopalswamy et al. 2001). However, there is still some controversy concerning the exact relationship between the metric type II radio emissions observed by ground-based observatories and the associated coronal mass ejections (CMEs). Direct positional comparisons between type II sources observed by radioheliographs and coronal transients have often shown that the type II sources may be produced well behind the CME leading edges (Wagner & MacQueen 1983; Gary et al. 1984). These observations seem to support the idea that the observed radiation is produced by a blast wave initiated during the impulsive phase of a flare and travelling through the ejected material. As a consequence, the outward propagation of the shock would not be physically coupled to the coronal transient dynamics.

Although radioheliographs can provide information on the shock location, observations of coronal radio bursts with such instruments are still scarce and affected by a variety of influences, such as projection effects, refraction by the Earth's ionosphere and effects of propagation in the lower corona. In absence of radioheliograph observations, the association between CME dynamics (inferred from coronagraphic white-light images) and shock dynamics (inferred from the observed frequency drift of the type II emission in radio dynamics spectrographs) can be deduced from a correlation study of the two speeds. Reiner et al. (2001) found no obvious correlation between shock speeds derived from metric type II radio bursts and the corresponding CME speeds, while Shanmugaraju et al. (2003) found a weak correlation over a wider sample. A different analysis by Claßen & Aurass (2002) suggested that the metric type II radio bursts observed during the rising phase to solar maximum may originate either at flare-related blast wave shocks, or at shocks driven by the leading edge, the internal parts or the flanks of CMEs.

The above studies included events far from the limb that could be strongly affected by projection effects. Moreover, they were based on type II heights derived from a specific coronal density model (e.g. Newkirk 1961) and not upon actual measurements of density in the type II source regions. The error on the calculation of the shock speed is strongly dependent on the functional form of the electron density-height model being used, so that a correct estimate of the coronal density profiles is essential in order to study the relationship between CME and

Send offprint requests to: S. Mancuso,
e-mail: mancuso@to.astro.it

Article published by EDP Sciences and available at http://www.aanda.org or http://dx.doi.org/10.1051/0004-6361:20031510

shock dynamics. Actually, it could be misleading to apply an inconsistent coronal density model to compare the dynamics of the CME/shock events. In fact, the coronal density profiles of the background pre-shocked plasma can vary as much as an order of magnitude during the rising phase to solar maximum corresponding to substantial variations of the derived speeds (Mancuso et al. 2003).

In this paper, we will consider a subset of twenty-nine events from a sample of thirty-seven type II events analyzed by Mancuso et al. (2003). This subset of events was found to be temporally associated with CME eruptions. The remaining eight events did not display concomitant transient activity or their association with CMEs was not clear. It is also possible that the associated transient activity for some of these events was below the sensitivity of the instruments. A brief description of the observations and analysis of the data will be presented in Sect. 2. In Sect. 3 we will interpret the observed correlation between type II and CME activity in terms of emission originating from the top or the flanks of a bow/piston shock surface, extending just above the CME leading edge surface. In Sect. 4 we will discuss the results. Finally, our conclusions will be drawn in Sect. 5.

2. Observations and data analysis

The metric type II radio bursts that were used for our study period were collected by examining the Solar Geophysical Data (SGD) bulletins published by NOAA, U.S. Department of Commerce. These radio bursts were observed by ground-based radio telescopes at various observatories from around the world. Out of all metric type II radio bursts observed during the period between March and December 1999, we selected 29 events associated with CME events that occurred close to the east- or west-limb and for which we could extract information on the density profiles of the streamers above the associated active regions.

Ultraviolet coronal observations were obtained from the daily synoptic program of the UltraViolet Coronagraph Spectrometer (UVCS) telescope (Kohl et al. 1995) aboard the Solar and Heliospheric Observatory (SOHO) spacecraft. In the 1999 UVCS synoptic program, radial scans were made at six heliocentric heights (from 1.5 up to 3.5 $R_\odot$), moving the slit around the disk in steps of 45°, thus providing radial profiles of the Lyα and O VI line intensities over the entire corona. The UVCS diagnostics for the coronal electron density profiles of the pre-shocked plasma used in this work have been explained in Mancuso et al. (2003) and will not be repeated here. Since synoptic UVCS observations were made almost daily during 1999, we were generally able to evaluate the electron density profiles of the streamers above active regions associated with the radio bursts just a few hours before the shock passage. For convenience, the observed density profiles were fitted with the function $n_e(r) = \alpha \times 10^{\rho/r}$, where r is the radial distance in units of solar radii. The functional form of the above profile is similar to the Newkirk (1961) density model. The two parameters α and ρ were estimated by fitting the observed density profiles between 1.5 and 2.3 $R_\odot$.

The dynamics of the shocks were determined by examining the slowly drifting bands of emission in the radio dynamical spectra. Type II burst radiation is in fact excited by fast mode MHD shock waves propagating outward through the corona and requires a coherent plasma emission mechanism near the local electron plasma frequency $f_{pe}[\mathrm{Hz}] = 8978\sqrt{n_e[\mathrm{cm}^{-3}]}$ and its second harmonic. The heights corresponding to the observed plasma frequencies in the radio dynamical spectra were obtained by inserting the fitted coronal density profiles in the formula for f_{pe} and solving for r, yielding $r(t) = \rho/\log\left\{[f_{pe}(t)/(8978\sqrt{\alpha})]^2\right\}$. The shock speeds $v_S = \frac{dr}{df}$ were consequently estimated by a linear regression of the heights in function of time. These estimates assume that the speed of the shock does not vary much from 1.5 to 2.3 $R_\odot$.

The dynamics of the CMEs related to the shocks examined in this study were inferred from the Large Angle and Spectrometric Coronagraph (LASCO) (Brueckner et al. 1995) C2/C3 height-time measurements available from the online SOHO/LASCO CME catalog (Yashiro et al. 2002). The CME speeds were estimated by assigning 10% error bars to the measured CME heights in each of the coronagraph images and performing linear (constant speed) or quadratic (constant acceleration) weighted least squares fit to the height-time trajectories. The CME speeds were estimated with linear fits only when the number of data points available was too small for a quadratic fit to be reliable. No attempt was made to correct for projection effects since all events originated near to the Sun's limb (typically within 30° from the limb). In general, we confirmed the source positions using the daily movies of EUV images obtained by the Extreme-ultraviolet Imaging Telescope (EIT) (Delaboudiniere 1995) on board SOHO.

Table 1 lists the details of the 29 CME/shock events used in this study. The association of type II burst data with solar flares and CMEs was inferred according to closeness in time. The first three columns give information on the type II burst date, start/end UT time, and speed (with 1σ error). The next three columns provide the flare information (timing, position and intensity) obtained from the listings of the National Geophysical Data Center (NGDC). Finally, the last four columns give information on the CMEs: the time and height (in $R_\odot$) of first appearance in the field of view of the LASCO coronagraph, the central position angle, and the speed derived from linear or quadratic fits.

Figure 1 shows multiwavelength observations related to the August 4, 1999 event. The top of Fig. 1 displays a sequence of three composite running difference images of a CME eruption from EIT 195 Å (innermost), and LASCO C2 (outermost) obtained by subtraction of two successive images. The bottom left of Fig. 1 shows a meter-wave dynamic spectrum for the same event. The features drifting to lower right (starting at about 05:52 UT) represent type II fundamental and harmonic emission moving into the solar wind through a decreasing density (hence a decreasing plasma frequency). The bottom right of Fig. 1 displays the LASCO C2/C3 height-time measurements for the same event. The solid line is a weighted least squares, quadratic fit of the CME's leading edge measurements (squares with error bars) in the plane of the sky, while

Table 1. Parameters of the CME/flare/type II burst events observed between March and December 1999. See the text for further explanation.

Type II burst			Flare			Coronal Mass Ejection			
Date	Start End (UT)	$v_{\text{type II}} \pm 1\sigma$ (km s^{-1})	Onset Peak (UT)	Location (°)	Magn.	1st C2 App. (UT)($R_\odot$)	PA (°)	Width (°)	$v_{\text{CME,fit}}$ (km s^{-1})
Mar. 08	06:38 06:51	620 ± 114	06:30 06:37	S24 E93	M 2.6	06:54 (2.30)	115	80	717
Apr. 03	23:06 23:17	385 ± 104	22:56 23:10	N29 E81	M 4.3	23:47 (5.11)	74	156	908
May 29	03:11 03:32	461 ± 39	03:04 03:15	S23 E62	M 1.6	03:26 (2.65)	81	135	762
Jun. 04	07:02 07:17	514 ± 68	06:52 07:03	N17 W69	M 3.9	07:42 (12.1)	289	150	2252
Jun. 11	00:39 00:49	527 ± 61	01:05 01:10	W limb	C 1.0	01:27 (4.78)	288	101	742
Jun. 11	11:15 11:31	1212 ± 290	11:07 11:57	E limb	C 8.8	11:26 (2.74)	35	181	1581
Jun. 23	05:45 05:55	619 ± 89	00:37 00:47	S12 W78	C 7.9	05:54 (2.80)	254	110	714
Jun. 30	09:37 09:42	482 ± 272	09:21 09:45	E limb	C 2.6	09:54 (2.99)	90	128	547
Jul. 09	00:33 00:46	312 ± 59	00:39 00:44	N19 E64	C 1.0	01:31 (3.33)	192	36	400
Jul. 10	00:00 00:12	473 ± 72	23:56 24:01	S14 E58	C 3.1	00:30 (2.82)	74	107	523
Jul. 11	13:22 13:26	591 ± 406	13:13 13:20	S21 W67	C 1.2	13:54 (2.96)	236	85	488
Jul. 12	18:40 18:51	590 ± 98	18:10 21:34	W limb	C 1.9	18:54 (2.52)	262	76	478
Jul. 16	15:54 16:25	720 ± 114	15:42 15:50	N43 W71	M 3.1	16:30 (4.72)	301	111	825
Jul. 19	08:40 08:44	672 ± 83	08:16 08:46	N18 E59	M 5.8	09:06 (3.51)	75	102	853
Jul. 21	09:14 09:18	804 ± 309	09:09 09:13	E limb	B 7.4	09:30 (2.54)	106	23	703
Aug. 04	05:51 05:58	536 ± 131	05:45 05:57	S16 W64	M 6.0	06:26 (2.31)	262	144	418
Aug. 06	16:40 16:46	1194 ± 157	16:28 16:36	S30 W85	M 1.8	18:42 (10.3)	257	69	906
Aug. 20	18:39 18:47	542 ± 130	18:25 18:29	S23 E66	M 1.2	18:50 (3.29)	84	94	712
Aug. 20	23:17 23:33	973 ± 145	23:03 23:08	S25 E64	M 9.8	23:26 (4.03)	95	76	1040
Aug. 21	16:52 17:01	991 ± 136	16:30 16:34	S25 E56	M 3.7	16:50 (3.40)	108	68	1214
Sep. 21	03:12 03:15	1066 ± 408	03:00 03:32	N19 W90	C 5.2	03:30 (4.48)	298	125	1492
Oct. 20	09:31 09:41	693 ± 94	09:25 09:29	S14 E78	C 2.2	10:06 (2.74)	93	51	475
Oct. 22	08:53 08:58	497 ± 251	09:10 09:16	N19 W76	C 4.8	08:50 (3.21)	300	73	585
Oct. 22	13:00 13:19	489 ± 88	14:04 14:07	N20 W76	C 3.4	13:27 (4.97)	305	118	644
Oct. 23	01:25 01:42	439 ± 70	00:48 01:07	W limb	C 2.7	01:27 (4.67)	305	143	1215
Oct. 26	21:30 21:50	434 ± 36	21:09 21:25	W limb	M 3.7	21:50 (2.68)	256	49	376
Oct. 27	13:25 13:38	551 ± 89	13:24 13:37	E limb	M 1.8	13:50 (2.53)	84	94	481
Nov. 27	05:02 05:08	559 ± 201	04:50 05:08	S13 W60	C 9.9	05:54 (2.63)	270	65	352
Dec. 29	09:35 09:39	549 ± 79	09:22 09:27	N22 W66	C 8.8	09:54 (3.04)	304	70	546

the dashed line is a weighted least squares, linear fit to the CME data. The type II burst inferred heights (stars) are also plotted. The in set shows the CME speed (solid and dashed lines) calculated from, respectively, the above quadratic and linear fits, together with the inferred shock speeds (stars with error bars). The onset time (diamond) and maximum time (triangle) of the associated flares are also indicated. We mention that extrapolation of the shock trajectories below 1.5 $R_\odot$ could be inaccurate since coronal density estimates were obtained only above 1.5 $R_\odot$ (the lower limit of the slit of UVCS) but only extrapolated at lower heights.

The August 4 event represents a particular case where both CME and shock dynamics match quite well. The shock speed, slightly higher than the CME speed, is suggestive of a bow/piston shock scenario (e.g. Vrsnak & Lulic 2000). In fact, the velocities of the shock and of the CME are similar, and the radio emission associated with the shock originates in proximity of the CME. However, for most of the events collected in our data set, the CME/shock dynamics turn out to be not correlated. Figure 2a displays the derived metric type II speed versus the corresponding CME speeds for all events. In general, we find that the shock speeds inferred from metric type II bursts correlate only marginally with the CME speeds (linear correlation coefficient $r = 0.45$). The probability to find the current result if the correlation coefficient were in fact zero (null hypothesis) is 1.4% ($P \sim 0.014$). We note that this outcome is in good

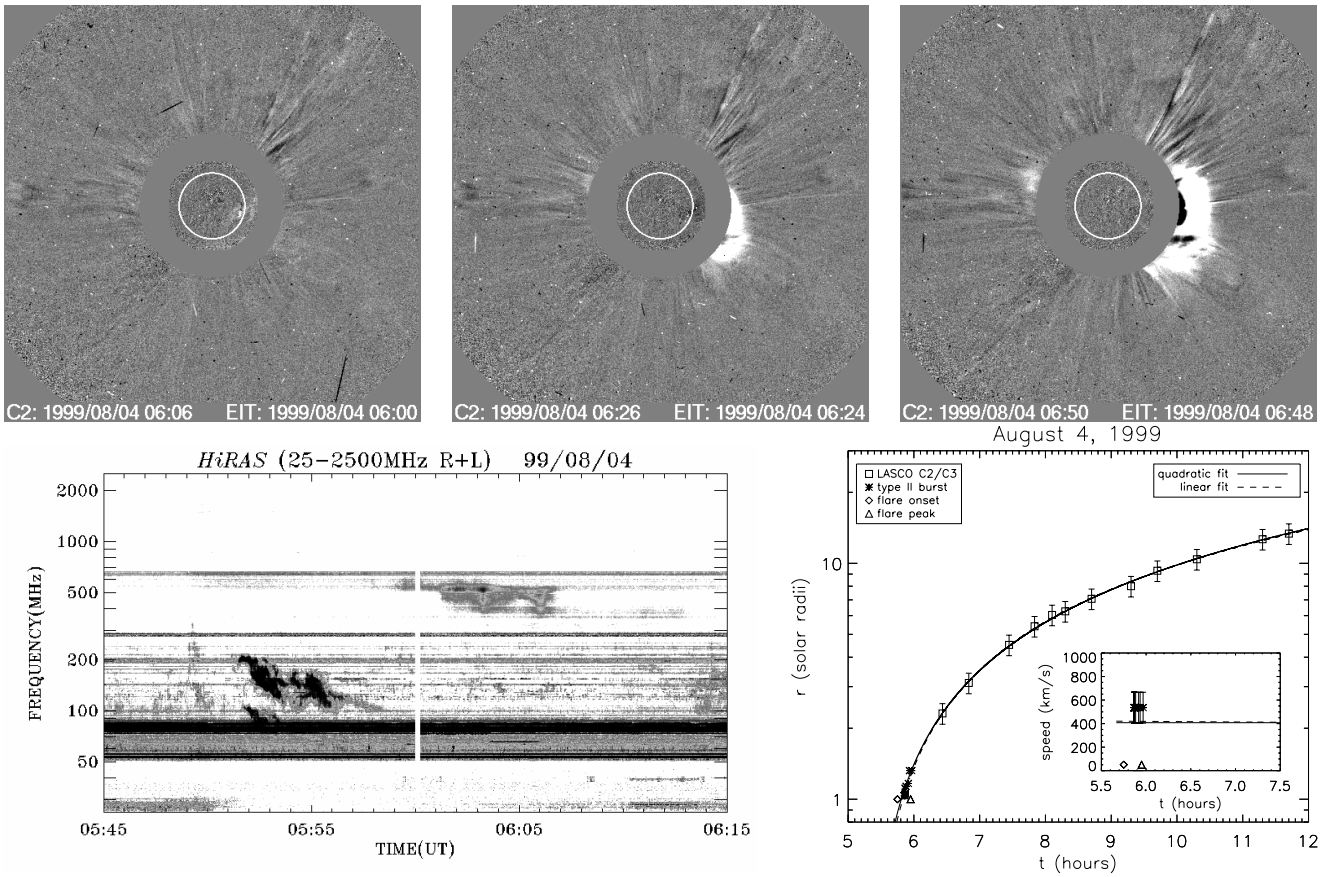

Fig. 1. The August 4, 1999 event. **Top:** sequence of three composite running difference images of the CME eruption from EIT 195 Å (innermost), and LASCO C2 (outermost) obtained by subtraction of two successive images. The observation times are indicated on each image. **Bottom left:** meter-wave dynamic spectrum for the same event over the time and frequency ranges shown (courtesy CRL Hiraiso). The features drifting to lower right (starting at about 05:52 UT) plot mark coronal disturbances moving through a decreasing density (hence a decreasing plasma frequency), i.e. upwards through the corona. **Bottom right:** height-time plot of the same event. The solid line is a least squares, linear fit of the CME measurements (squares with error bars) in the plane of the sky. The dashed line is a least squares, second-degree polynomial fit to the CME data. The type II inferred heights (stars) are also plotted. The inset shows the CME speed (solid and dashed lines) calculated from, respectively, the above linear and quadratic fits, and the inferred type II speeds (stars with error bars). The onset time (diamond) and maximum time (triangle) of the associated flares are also indicated.

agreement with the conclusions of Shanmugaraju et al. (2003) for a sample of 25 events, although it is at variance with the result of Reiner et al. (2001) that found $r = -0.07$ for a sample of only 10 events.

A simple correlation analysis of the CME/type II speeds although informative, is definitely not enough to confirm or refute the association between coronal transients and shocks and to cast more light on the (piston-driven or blast wave-driven) origin of the shocks. Together with the speed correlation, it is necessary to investigate the temporal coincidence between the CME/type II dynamics. For this purpose, we extrapolated the CME trajectories at 1.8 $R_\odot$ to show how these transients correlated in time with the associated type IIs. The result of this analysis is shown in Fig. 2b: all CME events occurred within forty minutes of the associated radio emission although most events displayed consistent negative delay times $\Delta t = t_{\mathrm{II},1.8\ R_\odot} - t_{\mathrm{CME},1.8\ R_\odot}$, apparently at odds with the piston-driven scenario. In fact, of the 29 CME/type II events considered here, only three type II bursts appeared to precede the CME leading edge. For the remaining events, the type II source was lagging behind the leading edge of the CMEs.

The most direct interpretation of these results is a blast wave origin of most of the shocks in our sample from their accompanying flares. Such an interpretation could be corroborated by the fact that in many cases the extrapolated start time for the type II radio burst is near the time of maximum phase of the soft X-ray flare and that all the cases examined in this study were accompanied by high intensity flares (see Table 1). Recently, Hudson et al. (2003) claimed to have identified soft X-ray emission from a flare-induced blast wave, though they did not perform a detailed analysis of the radio signatures in their paper. Although the relationship between flares and type II radio burst is of great interest for the understanding of the shock origin, we will not investigate further this issue since it is not essential in the discussion we are going to propose. Thorough statistical analyses dealing with the above issue can be found elsewhere (e.g. Claßen & Aurass 2002; Shanmugaraju et al. 2003), while a discussion of the flare activity related to

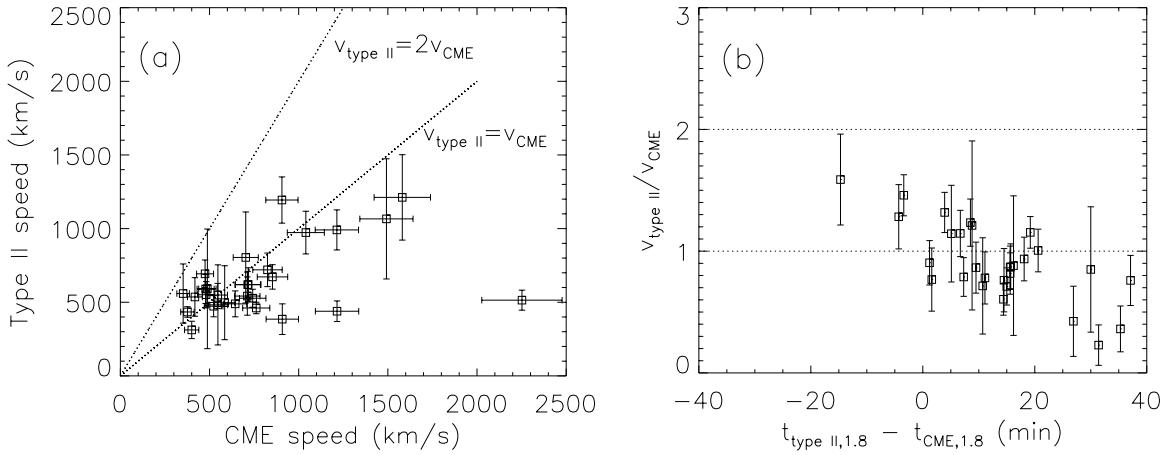

Fig. 2. a) Plot of the type II speeds versus CME speeds at 1.8 $R_\odot$ for all events and **b)** ratio between type II and CME speed versus delay times between CMEs and type IIs at 1.8 $R_\odot$.

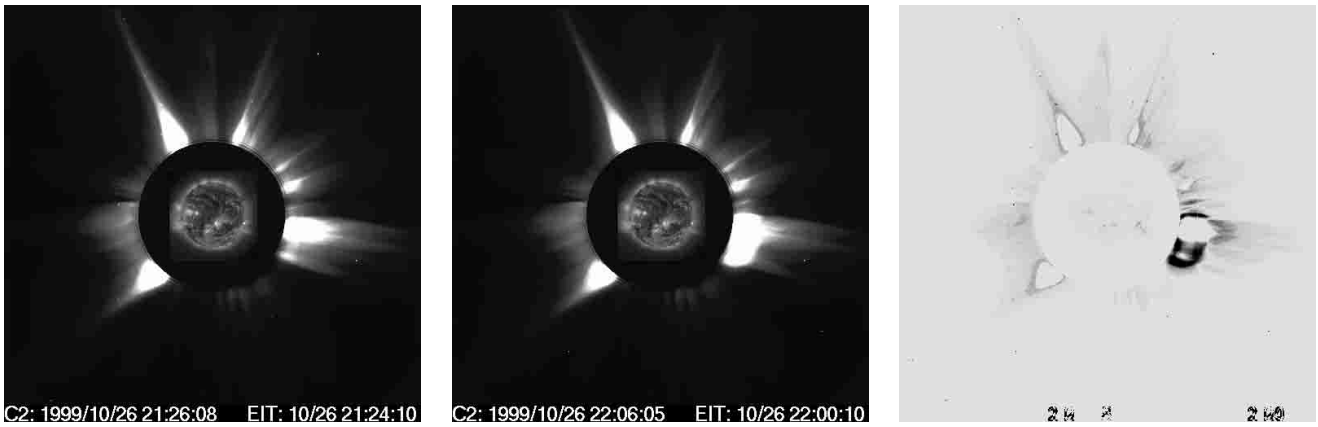

Fig. 3. Composite images from EIT 195 Å images (innermost), and LASCO C2 images (outermost). The LASCO C2 telescope recorded these images just before (left) and during (center) the CME eruption of October 26, 1999. The observation times are indicated on each image. The right panel displays a running difference image obtained by subtraction of the previous two images. By visual inspection, it is evident that the axes of symmetry of the CME expanding cone and of the streamer do not coincide.

the CME/shock dynamics will be the subject of a next paper (Mancuso et al., in preparation). It is however our intention to propose an alternative interpretation for the observed results, in order to stimulate further insight on this topic.

While admitting that a blast wave origin explanation for most events in our sample could still be viable, we will adopt an Occam's Razor approach and assume that all coronal shock waves (like their interplanetary counterparts) are driven by coronal transients. For this purpose, we will build up a model that attempts to solve the observed discrepancy between the CME/type II dynamics based on geometric effects, assuming that the radio emission comes from the top or the flanks of a bow/piston shock surface.

3. Model

Coronal mass ejections often appear to be composed of a bright leading looplike structure followed by a dark cavity and a bright core of denser prominence material. The roughly circular cavity might be interpreted as the sky-plane projection of a spherical plasmoid disconnected from the solar surface or a loop-like flux rope. In the case of a piston-driven shock, the CME dynamics through the ambient solar wind must satisfy the condition $v_{CME} > v_W + v_F$, where v_W is the solar wind flow speed, $v_F = \left\{\left[(v_A^2 + c_S^2) + \sqrt{(v_A^2 + c_S^2)^2 - 4v_A^2 c_S^2 \cos^2\theta}\right]/2\right\}^{1/2} \leq \sqrt{v_A^2 + c_S^2}$ is the coronal MHD fast-mode speed along the line of propagation of the CME, v_A is the Alfvén speed, c_S is the sound speed, and θ is the angle between the magnetic field and the direction of propagation. The strength of a MHD fast-mode shock in the corona can vary because of the inhomogeneous distribution of the coronal Alfvén speed (Mann et al. 2003) and be very much enhanced on those part of the wave front that encounter low-Alfvén speed structures (Kahler & Reames 2003). The axes of coronal streamers can be identified as the appropriate low-v_A structures having high density and comparatively weak magnetic field.

During the solar maximum phase there is a considerable chance that the wavefront sweeps up along the axes of streamers. In Fig. 3, we show composite images of EIT 195 Å (innermost), and LASCO C2 (outermost) for the CME event of October 26, 1999. The LASCO C2 telescope recorded these

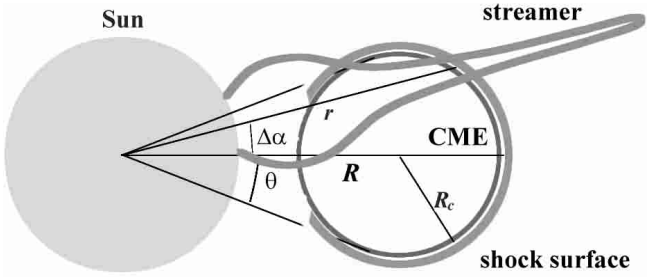

Fig. 4. Schematic picture showing our model of the shock surface expansion in front of the CME leading edge. $\Delta\alpha$ is the angle between the axis of symmetry of the CME expanding cone and the axis of the streamer, where the shock strengthens.

images just before (left) and during (center) the CME eruption. The right panel displays a running difference image obtained by subtraction of two successive white-light images. From the latter image, we notice that the CME expands above a streamer structure but that its expansion is not symmetrical around the axis of the streamer. In fact the axes of symmetry of an expanding CME and of the streamer over which the transient propagates are generally offset by a certain angle $\Delta\alpha$. The bow/piston shock strength will be then enhanced along a direction (corresponding to the low-v_A streamer axis) that forms an angle $\Delta\alpha$ different from zero with respect to the axis of symmetry of the expanding CME. This direction would be the best candidate location for the type II radio emission during the transient's propagation.

In the projection of the sky, most of the CME events observed near the limb by LASCO are similar to cone-shaped blobs with nearly constant angular widths as a function of height. In order to allow for a quantitative analysis, we model a bow/piston shock surface that propagates hemispherically just above a conically expanding bubble-type CME leading edge. Figure 4 shows a schematic illustration of the expansion of the shock surface above such a bubble-type CME ejected from the Sun's west limb. The axis of symmetry of the expanding cone does not coincide with the axis of symmetry of the overlying streamer but they form an angle $\Delta\alpha$. The bow shock surface is supposed to expand at a fixed angle 2θ, that will be assumed to coincide with the observed CME sky-plane width obtained from the online LASCO catalog and listed in Table 1.

From geometrical consideration, a point r on the hemispherical shock surface in the plane of the sky at the time t is determined by solving the following quadratic equation for $r(t)$:

$$r(t)^2 + 2r(t)[R_c(t) - R(t)]\cos\Delta\alpha + [R_c(t) - R(t)]^2 - R_c(t)^2 = 0 \quad (1)$$

and taking the positive root. Here $R(t)$ is the distance of the leading edge measured from the center of the Sun at the time t at the point where the axis of symmetry of the cone intersects the shock surface. The radius $R_c(t)$ of the expanding bubble at the time t is given by $R_c(t) = R(t)\sin\theta/(1+\sin\theta)$, where θ is half the angle of the cone (see Fig. 4).

4. Results and discussion

In principle, the angle $\Delta\alpha$ that quantifies the inclination of the streamer axis with respect to the axis of symmetry of the expanding CME/bow shock cone could be roughly estimated by inspection of the white-light images. However, this angle would be necessarily underestimated by an unknown factor, due to our lack of information on the streamer geometry along the line of sight. Even if we knew for some reason the streamer inclination with respect to the line of sight, a further complication would be given by the fact that the geometry and actual extension of the shock surface above the coronal transient is not known. Actually, the geometry of the leading shock front for CMEs propagating at superAlfvénic speeds remains yet to be determined. In fact, due to the anisotropy induced by the magnetic field, MHD shock surfaces can have complicated structures (e.g. de Sterck & Poedts 1999). The angle $\Delta\alpha$ will be therefore our only free parameter (ranging from 0 to θ) and will be adjusted in order to minimize the time lag between the shock and CME leading edge along the streamer's axis direction.

Figure 5 shows model results corresponding to four of the events listed in Table 1 applied to the LASCO height-time measurements. The lines and symbols are the same as used in Fig. 1e. In addition, Fig. 5 also provides the trajectory of that portion of the shock surface inclined by an angle $\Delta\alpha$ with respect to the axis of symmetry of the expanding cone (dotted line) corresponding to the location of the type II emission. The fits were obtained finding the angle correction $\Delta\alpha$ that minimizes the time lag between the shock and CME leading edge at a (projected) height of 1.8 $R_\odot$ along the streamer's axis direction, and assuming that the shock surface is just wrapped around the CME leading edge.

An important model result is that the introduction of the angle correction $\Delta\alpha$ improves considerably the correlation between shock and CME speeds, as shown in Fig. 6a. In fact, the linear correlation coefficient increases from the original $r = 0.45$ (obtained without angle correction) to $r = 0.81$ (compare Fig. 2a and Fig. 6a). Since the p-value is $P < 0.0001$, we have now enough evidence to reject the null hypothesis. As for the type II speeds, they all turn out to be at least not lower (within the errors) than the associated projected CME speeds at the location of type II emission. This latter result is outstanding and, together with the above strong correlation, matches perfectly the bow/piston driven shock scenario. By inspection, we notice that the type II speeds do not generally exceed the CME speeds by a factor of two. The histogram in Fig. 7 shows that in most cases, good fits were obtained only in the limit $\Delta\alpha \to \theta$, maybe suggestive of particular favorable conditions involved in the generation of the type II radiation for these events. In particular, for angles $\Delta\alpha \sim \theta$, the shock surface is almost parallel to the direction of the radial component of the magnetic field, favoring a mechanism of shock drift acceleration at quasi-perpendicular shocks (Holman & Pesses 1983). This latter mechanism is often invoked for the acceleration of the energetic electrons responsible for type II emission.

Although our model must be considered as an instructing exercise due to the oversimplification of the real geometry involved in each event, our results do suggest that the

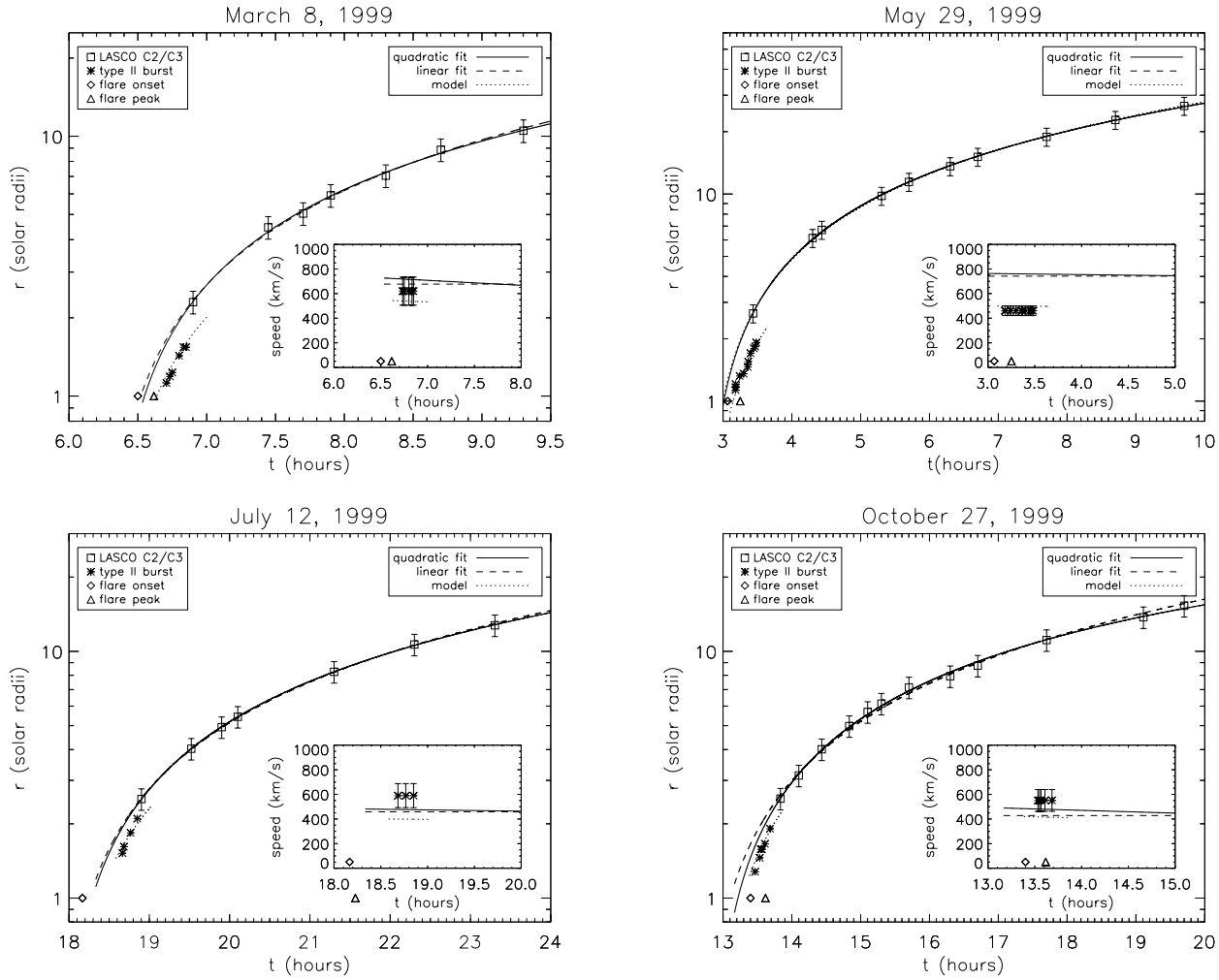

Fig. 5. Same as for Fig. 1e but for the events of March 3, May 29, July 12, and October 27, 1999. Model trajectories of the type II bursts are represented by dotted lines.

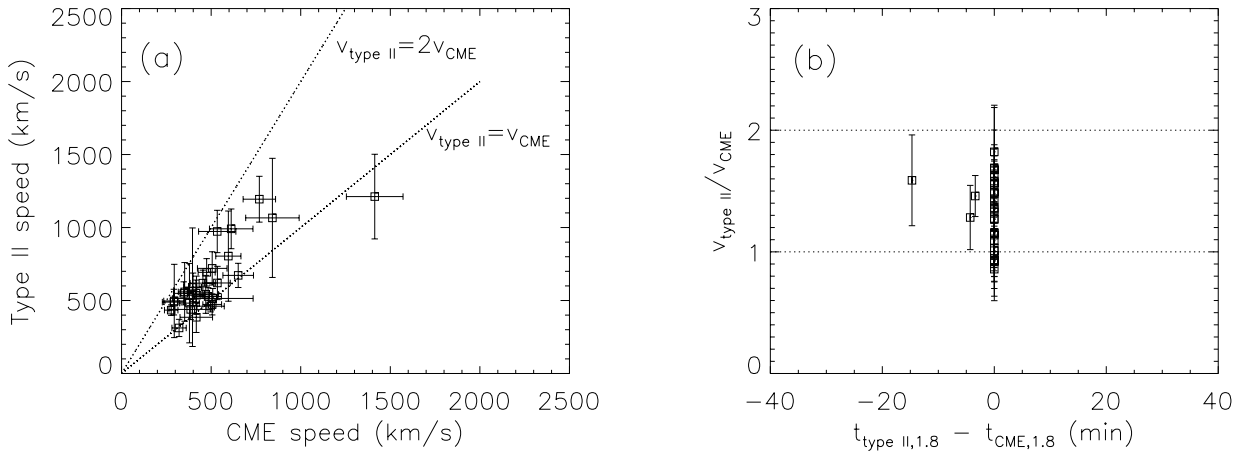

Fig. 6. Same as for Fig. 2, but adopting the angle correction $\Delta\alpha$ that minimizes the time lag between the type II and CME leading edge at a (projected) height of 1.8 $R_\odot$ along the streamer's axis direction.

apparent discrepancy of the CME and shock dynamics could be masked by purely geometrical effects. In other words, it is clear that under reasonable geometrical conditions, there could be a similarity between the dynamics of the type II emissions and CME leading edges. This close association appears to validate a bow/piston shock origin interpretation even when, apparently, the type II radio emission lags the CME by tens of minutes and its speed is much lower than the one of the associated transient. If this interpretation is correct, we expect narrow CMEs to be less efficient in generating type II emission since, due to their limited extension, they would have less chance to intersect nearby streamer structures.

With respect to the above discussion, we must emphasize that the blast wave interpretation for the events in our sample is not refuted by our model, but simply questioned. A thorough analysis of the correlation between streamer positions and type II radio emission locations for a sample of events using radioheliograph observations would easily validate or refute the above interpretation. Finally, we mention that strong positive accelerations at lower heights below the LASCO C2 field of view could affect the relationship between CME and shock dynamics. In fact, the linear and quadratic extrapolation methods used here are probably inaccurate near the surface of the Sun where they predict a finite speed, while a significant acceleration is certainly present before the CME acquires the speed inferred by coronagraphic images (St. Cyr et al. 1999; Neupert et al. 2001; Zhang et al. 2001). Evidently, a combination of both geometry effects and strong positive accelerations affect in some important way the CME/shock relationship. A detailed analysis of the effects of the acceleration below 2 $R_\odot$ applied to a subset of CME/shock events from our sample will be presented in a forthcoming paper (Mancuso et al., in preparation).

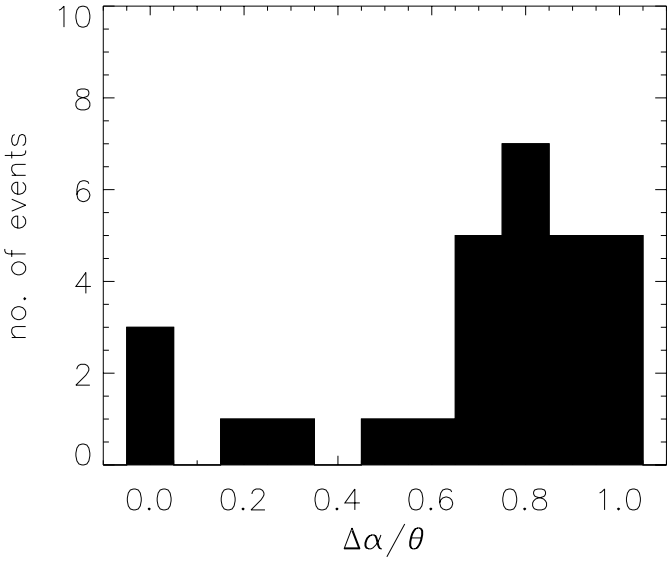

Fig. 7. Ratio between the angles $\Delta\alpha$ and θ defined in the paper. The histogram shows that in most cases, good fits were obtained only in the limit $\Delta\alpha \rightarrow \theta$, maybe suggestive of particular favorable conditions involved in the generation of the type II radiation for these events.

5. Summary and conclusions

A model has been applied to a set of CME/shock events in order to study the relationship between the dynamics of type II radio emissions and their temporally associated CMEs. Although the blast wave nature of the shocks in our sample cannot be discarded on the basis of our model, we found that the apparent discrepancy between the dynamics of the CME/shock events can be essentially unravelled by simple geometrical effects. More specifically, we showed that all shocks in our sample that were found to be clearly associated with CMEs could be bow/piston driven by the top or the flanks of expanding CMEs if appropriate geometrical considerations were taken into account. In conclusion, the good correlation between LASCO and type II dynamics obtained by accounting for a more accurate density versus height coronal profile, together with the strong and significant correlation obtained by allowing for effects of geometry suggest that a fairly large fraction of metric type IIs are actually CME-driven.

Notwithstanding the above, we would like to mention some major uncertainties that could affect our analysis. Firstly, it should be pointed out that metric radio observations and LASCO observations correspond to different spatial regimes, so that eventual accelerations below 2 $R_\odot$ would not be accounted for. Secondly, it must be remembered that our inferred densities represent the average on the pre-shocked plasma a few hours before the events. The dynamical nature of the active regions in the pre-flare phase and the reconfiguration of the magnetic fields could produce changes in the structure of the streamers in the period between the measurement of the density and the beginning of the flaring phase that could affect somehow our analysis. Thirdly, systematic errors and estimate uncertainties of some of the parameters involved in our density (and consequently speed) evaluation can affect our result in unpredictable ways (see Mancuso et al. 2002 for a discussion). Finally, the real geometry of the shock surfaces above the expanding CMEs is not known and has only been tentatively modelled by conically expanding hemispherical surfaces.

Acknowledgements. The CME catalog is generated and maintained by the Center for Solar Physics and Space Weather, The Catholic University of America in cooperation with the Naval Research Laboratory, and NASA. SOHO is a project of international cooperation between ESA and NASA. The Hiraiso Radio Spectrograph is operated by the Communications Research Laboratory, Japan.

References

Brueckner, G. E., Howard, R. A., Koomen, M. J., et al. 1995, Sol. Phys., 162, 357
Cane, H. V., Sheeley, N. R., & Howard, R. A. 1987, J. Geophys. Res., 92, 9869
Claßen, H. T., & Aurass, H. 2002, A&A, 384, 1098
Delaboudiniere, J.-P., Artzner, G. E., Brunaud, J., et al. 1995, Sol. Phys., 162, 291
de Sterck, H., & Poedts, S. 1999, A&A, 343, 641
Gary, D. E., Dulk, G. A., House, L., et al. 1984, A&A, 134, 222
Gopalswamy, N., Yashiro, S., Kaiser, M. L., et al. 2001, J. Geophys. Res., 106, 29219

Holman, G. D., & Pesses, M. E. 1983, ApJ, 267, 837
Hudson, H. S., Khan, J. I., Lemen, J. R., Nitta, N. V., & Uchida, Y. 2003, Sol. Phys., 212, 121
Kahler, S. W., & Reames, D. V. 2003, ApJ, 584, 1063
Kohl, J. L., Esser, R., Gardner, L. D., et al. 1995, Sol. Phys., 162, 313
Mancuso, S., Raymond, J. C., Kohl, J., et al. 2002, A&A, 383, 267
Mancuso, S., Raymond, J. C., Kohl, J., et al. 2003, A&A, 400, 347
Mann, G., Klassen, A., Aurass, H., & Claßen, H.-T. 2003, A&A, 400, 329
Neupert, W. M., Thompson, B. J., Gurman, J. B., & Plunkett, S. P. 2001, J. Geophys. Res., 106, 25215
Newkirk, G. J. 1961, ApJ, 133, 983
Reiner, M. J., Kaiser, M. L., Gopalswamy, N., et al. 2001, J. Geophys. Res., 106, 25279
Shanmugaraju, A., Moon, Y.-J., Dryer, M., & Umapathy, S. 2003, Sol. Phys., 215, 161
St. Cyr, O. C., Burkepile, J. T., Hundhausen, A. J., & Lecinski, A. R. 1999, J. Geophys. Res., 104, 12493
Vrsnak, B., & Lulic, S. 2000, Hvar Observatory Bulletin, 24, 17
Wagner, W. J., & MacQueen, R. M. 1983, A&A, 120, 136
Yashiro, S., Gopalswamy, N., Michalek, G., et al. 2002, Am. Geophys. Union, Spring Meeting
Zhang, J., Dere, K. P., Howard, R. A., et al. 2001, ApJ, 559, 452